Volume 1 | Number 1 | Jan 2013 | Pages 1–100

Dalton Transactions

An international journal of inorganic chemistry
www.rsc.org/dalton

ROYAL SOCIETY OF CHEMISTRY

This is an *Accepted Manuscript*, which has been through the Royal Society of Chemistry peer review process and has been accepted for publication.

Accepted Manuscripts are published online shortly after acceptance, before technical editing, formatting and proof reading. Using this free service, authors can make their results available to the community, in citable form, before we publish the edited article. We will replace this *Accepted Manuscript* with the edited and formatted *Advance Article* as soon as it is available.

You can find more information about *Accepted Manuscripts* in the **Information for Authors**.

Please note that technical editing may introduce minor changes to the text and/or graphics, which may alter content. The journal's standard **Terms & Conditions** and the **Ethical guidelines** still apply. In no event shall the Royal Society of Chemistry be held responsible for any errors or omissions in this *Accepted Manuscript* or any consequences arising from the use of any information it contains.

ROYAL SOCIETY OF CHEMISTRY

www.rsc.org/dalton

Polymer *versus* phosphine stabilized Rh nanoparticles as components of supported catalysts:

implication in the hydrogenation of cyclohexene model molecule

M. Ibrahim,[a,b] M. A. S. Garcia,[c] L. L. R.Vono,[a,b,c] M. Guerrero,[a,b] P. Lecante,[d] L. M. Rossi,*[c] and K. Philippot*[a,b]

[a] *CNRS, LCC (Laboratoire de Chimie de Coordination), 205 route de Narbonne, BP 44099, F-31077-Toulouse Cedex 4, France*
[b] *Université de Toulouse, UPS, INPT, F-31077-Toulouse Cedex 4, France*
[c] *Department of Fundamental Chemistry, Institute of Chemistry, University of São Paulo, PO Box 26077, 05513-970, São Paulo, SP, Brazil*
[d] *CNRS UPR 8011; CEMES (Centre d'Elaboration des Matériaux et d'Etudes Structurales) 29 rue Jeanne Marvig, F-31055 Toulouse, France*
* karine.philippot@lcc-toulouse.fr

Graphical abstract
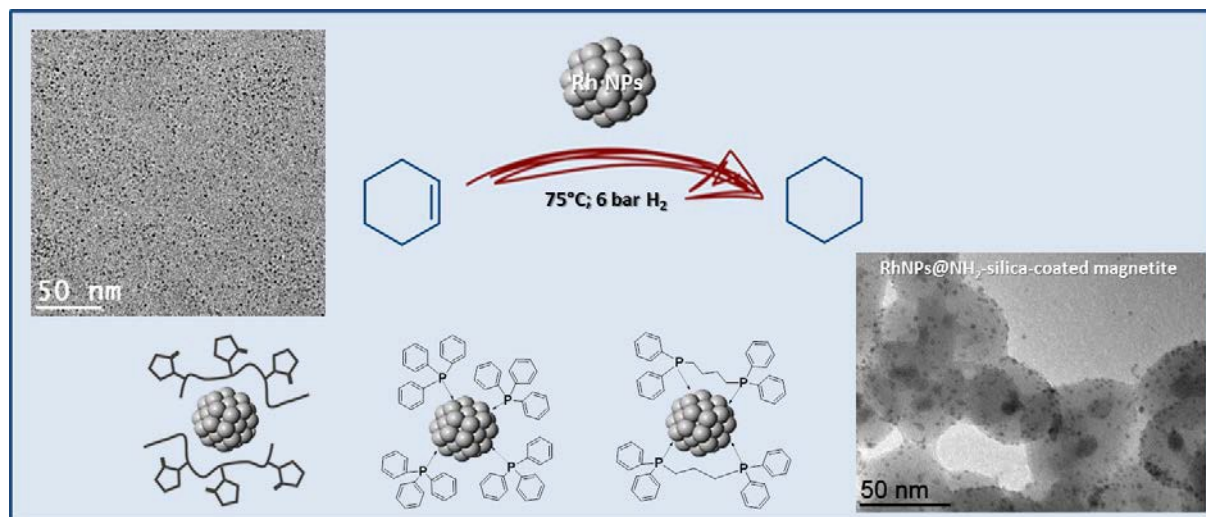
Influence of stabilizers on the catalytic performance of small rhodium nanoparticles was studied through a model hydrogenation reaction.

Key-words

Abstract

The solution synthesis of rhodium nanoparticles (Rh NPs) was achieved from the organometallic complex $[Rh(\eta^3-C_3H_5)_3]$ in mild reaction conditions in the presence of a polymer (PVP), a monophosphine (PPh$_3$) and a diphosphine (dppb) as a stabilizer, leading to very small Rh NPs of 2.2, 1.3 and 1.7 nm mean size were formed, with PVP, PPh$_3$ and dppb, respectively. The surface properties of these nanoparticles were compared using a model catalysis reaction namely, hydrogenation of cyclohexene, first in colloidal conditions and then in supported conditions after their immobilization onto an amino functionalized silica-coated magnetite support. PVP-stabilized Rh NPs were the most active catalyst whatever the catalytic conditions as the result of a strong coordination of the phosphine ligands at the metal surface that blocks some surface atoms even after several recycles of the supported nanocatalysts and limit the reactivity of the metallic surface.

Introduction

Metal nanoparticles of diverse compositions are intensively investigated given their unique properties and possibility of widespread applications in domains as different as biology, medicine, microelectronics, optics or catalysis to cite only a few. [1,2,3] In the field of catalysis, metal nanoparticles are interesting materials for two main reasons that are their high number of surface atoms and their borderline position between homogeneous and heterogeneous catalysts. [4] These characteristics are expected to provide to metal nanoparticles better catalytic performances by taking benefit of properties close to those of both molecular complexes and metallic surfaces. Nowadays nanocatalysis is recognized as a full part in the vast domain of catalysis. [5,6,7] With the aim to find novel and more performant catalysts in terms of reactivity and selectivity to develop more efficient and eco-compatible ways for chemical production, nanocatalysis presents several advantages. [8]

Given that numerous heterogeneous catalysts are constituted of metal particles often grafted onto a support, the relevance of metal nanoparticles has been known for a long time.[9,10] However, the use of ligands has often been considered as detrimental to the reactivity of metal nanoparticles because their presence can limit the access of reactants to the metallic surface and are mostly seen as poisons. Consequently, a calcination step is often applied for the preparation of heterogeneous catalysts to eliminate the organic portion. However, in the past two decades, a renewed interest has been directed towards ligand-stabilized metal nanoparticles and a lot of research is devoted to the synthesis of functionalized nanocatalysts by playing with ligands with the aim to take benefit from them.[11] This is because the use of ligands makes it possible to have nanoparticles whose surface metal atoms are modified in a way close to metal centers in homogeneous catalysts for which ligands are of paramount importance both for the stability and properties of metal complexes. Ligands give the possibility to tune the surface properties of metal nanoparticles through electronic or steric effects. In addition, ligand-stabilized nanoparticles can be investigated in catalysis both in solution and in supported reaction conditions.[12] The challenge is to find ligands able to stabilize well-defined nanoparticles while controlling accessibility at the metal surface and orientating their reactivity.[13] The study of the influence of ligands on catalytic activity has been less studied than the facet dependency but nice results illustrate well this important point.[14,15,16,17]

In this context, colloidal chemistry that allows readily, fine-tuning of the size, shape, structure and composition of metal nanoparticles is a powerful approach.[18] Among other methods, the use of organometallic complexes as the metal source has been proven to be an efficient way to prepare well-controlled nanoparticles of noble metals or others in organic or aqueous solutions in the presence of coordinating ligands as stabilizers.[19] The control of composition, the narrow size distributions and the clean surface states obtained for the particles, allow studying the influence of the stabilizing ligands on the nanocatalyst properties and to determine the most appropriate ones depending on the target application. Among others, the coordination of the ligands at metallic

surfaces is an important parameter to study.[20] Regarding sustainable concerns, this method can also be applied for the preparation of supported nanocatalysts, by impregnation of the support from a colloidal solution or by direct decomposition of a metal complex in the presence of the chosen support.[21,22,23] Catalytic systems which can be recovered and reused to satisfy recycling and eco-conception objectives can thus be developed by this way.

Despite the fact that rhodium is a rare and costly metal, this noble metal has found many applications, particularly in hydrogenation and hydroformylation owing to its specific catalytic properties. This interest for rhodium catalysts concerns also the modern nanocatalysis area with the preparation of colloidal suspensions of rhodium nanoparticles,[24,25,26] mainly by reduction of rhodium salts in water,[27,28] or organic phase,[29] for studies in liquid phase or for the design of supported nanocatalysts[29,30,31,32] but the influence of ligands on Rh NP surface properties is not often discussed. The organometallic approach for the synthesis of Rh NPs is not usual in the literature with only a few reports [33,34,35,36,37,38,39,40,41] but its interest to allow fundamental studies in nanocatalysis has been shown.

We describe hereafter the synthesis and the characterization by state-of-the-art techniques of polymer and ligand (phosphines)-stabilized rhodium nanoparticles using organometallic chemistry tools as well as a comparative study of their catalytic activity both in solution and in supported conditions through a model hydrogenation reaction.

Experimental

General and Materials

Chemicals were purchased as follows: THF and cyclohexane from Sigma-Aldrich and pentane from SDS; $RhCl_3.xH_2O$ from Johnson Matthey; PPh_3, $Ph_2P(CH_2)_4$-PPh_2, PVP (average molecular weight 40,000), $[CH_2$=$CHCH_2MgCl]$, $FeCl_2.4H_2O$, $FeCl_3.6H_2O$, oleic acid, NH_4OH, HCl, TEOS,

IGEPAL-CO520, (3-aminopropyl)triethoxysilane (APTES) and cyclohexene from Sigma-Aldrich or Acros-Organics, H_2 from Air Liquide. All operations concerning the synthesis of Rh precursor and Rh nanoparticles or the preparation of samples for characterization were carried out using standard Schlenk tubes and Fischer-Porter bottle techniques or in a glove-box (MBraun) under argon atmosphere. Solvents were purified before use by filtration on adequate column of a purification apparatus (MBraun) and handled under argon atmosphere. All reagents were used without purification except polyvinylpyrrolidone (PVP) which was dried under vacuum over P_2O_5 at 80°C for 3 days prior to use. Reagents and solvents were degassed before use according to a freeze-pump-thaw process.

Characterization Techniques

Transmission electron microscopy observations at low (TEM) and high resolution (HRTEM) were performed at the "Centre de microcaractérisation Raymond Castaing" in Toulouse (UMS-CNRS 3623). TEM grids were prepared by drop-casting of the crude colloidal solution in THF onto a holey carbon-coated copper grid under argon atmosphere in glove-box. TEM analyses were performed on a JEOL 1400 electron microscope operating at 120 kV with resolution point of 2 Å. HRTEM observations were carried out with a JEOL JEM 2010 electron microscope working at 200 kV with a resolution point of 2.5 Å and equipped with X-ray analysis PGT (light elements detection, resolution 135 eV).

Statistical size distributions were built by counting more than 200 non-touching particles and nanoparticle mean diameters were determined, by analyzing the TEM and HRTEM images with Image J tool software. The analyses were performed by assuming that the nanoparticles are spherical. Size distributions are quoted as the mean diameter ± the standard deviation.

Wide-angle X-ray scattering (WAXS) measurements were performed at CEMES-CNRS in Toulouse. Samples were sealed in 1.5 mm diameter Lindemann glass capillaries. The samples were

scattering intensity measurements were performed using a dedicated two-axis diffractometer. Radial

distribution functions (RDF) were obtained after Fourier transformation of the corrected and reduced

data.

Solution NMR

Nuclear Magnetic Resonance (NMR) solution experiments were performed at LCC-CNRS, Toulouse

on a Bruker (400 MHz or 500 MHz) spectrometer in deuterated chloroform ($CDCl_3$).

ICP OES and elemental analysis

ICP OES analyses were performed at LCC-CNRS in Toulouse using Thermo Scientific iCAP 6300

DUO spectrometer with a 3-channel, 12-roller pump, and a 27.12 MHz solid state RF plasma

generator. Mineralization of NPs was performed in aqua regia solution. Elemental analyses were

carried out with a PERKIN ELMER 2400 série II analyzer.

Gas chromatography

Gas chromatography analyses were performed with a Shimadzu GC-2010 Gas Chromatograph–

Flame Ionization Detector (FID) equipped with a capillary column Rtx-5 30 meter. The analyses

were performed under the following conditions: initial temperature 50 °C, rate 10 °C min^{-1} and final

temperature 150 °C.

Synthesis of [Rh(η^3-C$_3$H$_5$)$_3$] organometallic complex

[Rh(η^3-C$_3$H$_5$)$_3$] organometallic complex was prepared according to a slightly improved method

from the literature starting from rhodium trichloride $RhCl_3.xH_2O$ and allylmagnesiumchloride

[CH$_2$=CHCH$_2$MgCl].[42] A THF solution (140 mL) of $RhCl_3.xH_2O$ (1.5 g; 7.2 mmol) was reacted

under inert atmosphere and vigorous stirring with allylmagnesiumchloride (36 mL of a THF solution

at 2 mol.L^{-1}; 71.6 mmol) at -10°C for 1 h and then, 16 h at 10°C. During this period of time, the solution passed from red to yellow color. Evaporation of THF led to a solid that was dissolved in pentane leading to a yellow solution. After filtration on celite, pentane was evaporated under vacuum and the yellow solid obtained purified by sublimation at 40°C. Yellow crystals (660 mg) of [Rh(η^3-C$_3$H$_5$)$_3$] were collected with a yield of 41% and kept under argon atmosphere at low temperature.

^{1}H NMR (CDCl$_3$): 1.63 ppm, *dd*, 4H^a, J$_{HH}$=11Hz, J^{ab}=0.8Hz, C$\underline{H}_2$^{ab}, (C$\underline{H}_2$CHCH$_2$)$_2$; 2.62 ppm, *dd*, 2H^a, J$_{HH}$=11.7Hz, J$_{ab}$=1.32Hz C$\underline{H}_2$^{ab}, CH$_2$CHC$\underline{H}_2$; 2.77 ppm, *d*, 4$_H$^{a}, J$_{HH}$=6.62 Hz, CH$_2$^{ab}, (C$\underline{H}_2$CHCH$_2$)$_2$; 2.99 ppm, *d*, 2H^b, J$_{HH}$=6.65 Hz, CH$_2$^{ab}, C$\underline{H}_2$CHC$\underline{H}_2$; 3.96 ppm, *m*, 2H, C$\underline{H}$, (CH$_2$CHCH$_2$)$_2$; 5.35 ppm, 1H, C$\underline{H}$, CH$_2$C$\underline{H}$CH$_2$.

Elemental analysis: experimental (theoretical) %C: 48.05 (47.8); %H: 6.7 (6.7).

Synthesis of Rh NPs in solution

Rhodium nanoparticles were synthesized in THF solution from [Rh(η^3-C$_3$H$_5$)$_3$] organometallic complex and in the presence of a stabilizer either a polymer (polyvinylpyrrolidone, PVP) or a phosphine ligand (triphenylphosphine, PPh$_3$ or 1,4-bis(diphenyl)phosphinobutane, Ph$_2$P-(CH$_2$)$_4$-PPh$_2$, dppb) following the nanochemistry method developed in our group.

RhPVP NPs

150 mg of [Rh(η^3-C$_3$H$_5$)$_3$] (0.66 mmol) were introduced under argon atmosphere in a Fischer-Porter reactor. After 0.5 h under vacuum at r.t. and cooling to 193 K, a THF solution (150 mL) of PVP (680 mg; Rh/PVP=10% wt) was transferred under argon by canula. Then the reaction medium was let to warm up to r.t. before adding dihydrogen (3 bar). The reaction mixture was left under vigorous stirring at r.t. It turned from pale yellow to black color in a few minutes. After a reaction time of 16 h, a homogeneous black colloidal solution was obtained. Remaining dihydrogen was evacuated and the volume of the solution reduced to approximately 10 mL under vacuum before its transfer onto a

solution of deoxygenated cold pentane (100 mL). A black precipitate formed which was filtered and dried under vacuum giving rise to the Rh NPs embedded in PVP as a fine black powder (622.5 mg). These Rh PVP NPs were found to be stable with time when kept under argon atmosphere.

ICP OES analysis: Rh = 7.42 wt%.

RhPPh$_3$ NPs

150 mg of [Rh(η^3-C$_3$H$_5$)$_3$] (0.66 mmol) were introduced under argon atmosphere in a Fischer-Porter reactor. After 0.5 h under vacuum at r.t. and cooling to 193 K, a THF solution (150 mL) containing 174 mg of PPh$_3$ (0.66 mmol, [PPh$_3$]/[Rh] = 1) was added. Then the reaction medium was let to warm up to r.t. before adding dihydrogen (3 bar) and then put in an oil bath previously heated at 338 K. The reaction mixture was left at 338 K under vigorous stirring during 18 h. After this reaction time, a homogeneous black colloidal solution was obtained. After cooling at r.t., remaining dihydrogen was evacuated and the volume of the solution reduced to approximately 10 mL under vacuum before its transfer onto a solution of deoxygenated cold pentane (100 mL). A black precipitate formed which was filtered and dried under vacuum leading to the PPh$_3$-stabilized Rh NPs as a black powder (97.5 mg). RhPPh$_3$ NPs were found to be stable with time when kept under argon atmosphere.

ICP OES analysis: Rh = 27.1 wt%.

Rhdppb NPs

150 mg of [Rh(η^3-C$_3$H$_5$)$_3$] (0.66 mmol) were introduced under argon atmosphere in a Fischer-Porter reactor. After 0.5 h under vacuum at r.t. and cooling to 193 K, a THF solution (150 mL) containing 84.75 mg of dppb (0.20 mmol, [dppb]/[Rh] = 0.3) was added. Then the reaction medium was let to warm up to r.t. before adding dihydrogen (3 bar) and then put in an oil bath previously heated at 338 K. After cooling at r.t., remaining dihydrogen was evacuated and the volume of the solution reduced

to approximately 10 mL under vacuum before its transfer onto a solution of deoxygenated cold

pentane (100 mL). A black precipitate formed leading to the PPh$_3$-stabilized Rh NPs as a black

powder (66 mg). Rhdppb NPs were found to be stable with time when kept under argon atmosphere.

ICP OES analysis: Rh = 37.45 wt%.

Preparation of magnetic silica support

The magnetic support comprised of silica-coated magnetite NPs (FFSi) was prepared by reverse

microemulsion method and functionalized with amino groups (FFSiNH$_2$), as previously reported.[43]

Deposition of Rh NPs onto silica support

As a general procedure, a THF solution (40 mL) containing the Rh NPs (27 mg RhPVP NPs; 7.3 mg

RhPPh$_3$ NPs and 5.6 mg Rhdppb NPs) was added to 100 mg of the FFSiNH$_2$ support. The

suspension was left under vigorous stirring overnight at r.t. Stirring was stopped and the solid was

recovered by approximating a magnet to the reaction flask wall. The solvent was drained off

completely and the solid was then washed with ethanol before drying under vacuum leading to

RhPVP@FFSiNH$_2$, RhPPh$_3$@FFSiNH$_2$ and Rhdppb@FFSiNH$_2$ samples. This deposition protocol

was performed with 2 mg of rhodium metal for 100 mg of silica support. ICP OES measurement

allowed determining the metal content on the silica support after deposition of the nanoparticles. The

Rh content in the catalysts is for RhPVP@FFSiNH$_2$ NPs: 1.14 wt% Rh, for RhPPh$_3$@FFSiNH$_2$ NPs:

2.32 wt% Rh and for Rhdppb@FFSiNH$_2$ NPs: 1.44 wt% Rh.

Catalysis experiments

The hydrogenation reactions were carried out in a modified Fischer–Porter 100-mL glass reactor,

which was loaded with the catalyst (non-supported or supported Rh NPs) and cyclohexene under

inert atmosphere. The corresponding amounts are given in the tables. The reactor was connected to a

pressurized H$_2$ tank via a gas regulator, which was set to the required working pressure (typically, 6

bar). The pressure inside the reactor was maintained constant for the entire course of the reaction by leaving the reactor open to the H_2 supply tank. The temperature was maintained using an oil bath and a hot-stirring plate connected to a digital controller. The reactions were conducted under magnetic stirring (700 rpm) for the desired time. The fall in the H_2 pressure in the H_2 supply tank was monitored with a pressure transducer interfaced through a Novus field logger converter to a computer. The pressure *versus* time data were collected by the FieldChart Novus software. After each reaction was complete (hydrogen consumption ceased), the products were collected and analyzed by GC. From the hydrogen consumption curves, was obtained, for each reaction, the time required for the complete conversion (> 99 %, confirmed by GC). The catalytic activity was expressed in turnover frequency (TOF) determined using the data from the hydrogenation curves transformed into conversions and then into turnover numbers (mole of substrate converted per mole of catalyst). From the slope of the turnover numbers versus time curves at initial rates (typically <20 % conversion), the initial TOF, in h^{-1} was obtained. In recycling experiments, the magnetically recovered catalyst was dried in vacuum at room temperature before the addition of a new portion of substrate under inert atmosphere. The reactor was connected again to the H_2 gas supply tank and successive hydrogenation reactions were performed.

Results and discussion

The synthesis of phosphine-stabilized rhodium nanoparticles (Rh NPs) was performed following the organometallic approach. $[Rh(\eta^3-C_3H_5)_3]$ was chosen as metal source given previous results with this complex by our group in Toulouse.[44,45,46] A mono- and a diphosphine (triphenylphosphine, PPh_3 or 1,4-bis(diphenyl)phosphinobutane, $Ph_2P-(CH_2)_4-PPh_2$, dppb) were selected as stabilizers owing to our experience in nanochemistry with this kind of ligands with other metals.[47, 48] To investigate more deeply the influence of the phosphines on the nanoparticle surface properties, a polymer (polyvinylpyrrolidone, PVP) that is known to provide a steric stabilization and gives no or weak

interaction with the metal surface as shown previously while studying the magnetic properties of Co-PVP nanoparticles,[49] was also used to synthesize Rh nanoparticles for comparison purpose. The so-obtained nanoparticles were characterized by complementary techniques and investigated in model hydrogenation catalytic reaction with cyclohexene. Silica-supported nanocatalysts were also prepared to analyze the influence, if any, of the stabilizers on the catalytic properties of Rh NPs after their immobilization on a support and to facilitate the recovery of the catalyst.

Solution synthesis and characterization of Rh NPs

The synthesis of Rh NPs with the chosen stabilizers and their characterization by transmission electron microscopy (TEM) is presented on Figures 1 - 3. The decomposition of $[Rh(\eta^3\text{-}C_3H_5)_3]$ in THF solution under 3 bar of dihydrogen was carried out at room temperature (r.t.) in the presence of PVP. Reactions conditions were applied to obtain a metal amount of ca. 10-15 wt% as usually done in the group when using this polymer as a stabilizer. TEM analysis performed from fresh colloidal solution revealed the presence of well-dispersed and spherical RhPVP NPs of ca. 2.2 nm (Figure 1). These RhPVP NPs were easily isolated under the form of a dark grey powder by pentane precipitation with a metal content of 14.9 wt% as measured by ICP OES analysis. They display the fcc crystalline structure of rhodium metal as observed both by FFT treatment of the electron microscopy images and WAXS analysis (Figure 4, left). In real space (right), WAXS analysis confirmed the highly regular fcc character for these particles with a coherence length of ca. 2.2 nm in very good agreement with the mean diameter observed by TEM. Such agreement also indicates that in this sample NPs are single crystalline.
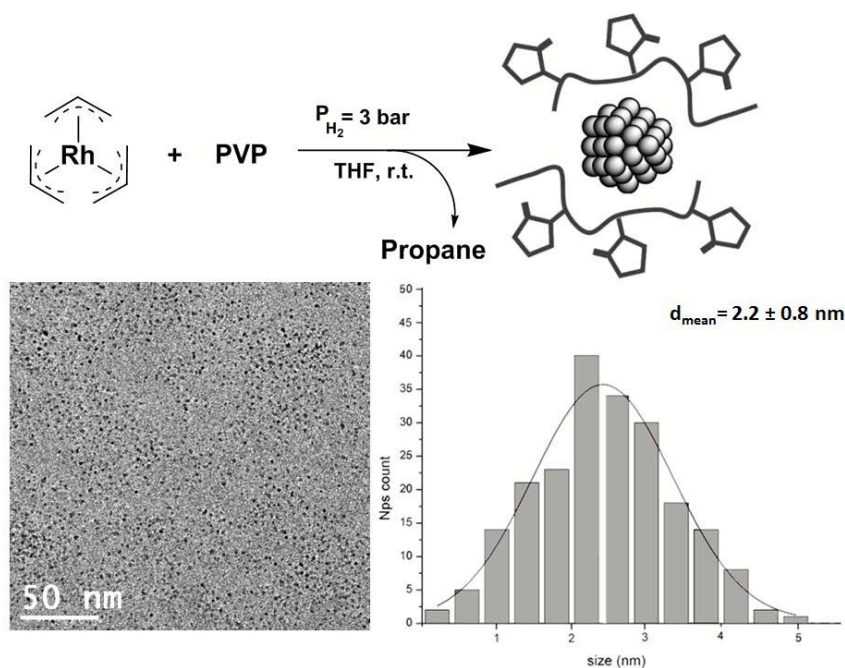
Figure 1. Synthesis, TEM image and size distribution histogram of PVP-stabilized Rh NPs

The synthesis of phosphane-stabilized Rh NPs was performed in a similar way as for RhPVP ones, but a temperature of 65°C was applied to get full decomposition of the metal precursor and obtain stable colloidal solutions NPs in a reproducible way. With PPh_3, a $[PPh_3]/[Rh]$ value of 1 was found to be the best ligand/metal ratio to obtain well-dispersed and well-controlled Rh NPs of ca. 1.3 nm (Figure 2). With dppb, a [dppb]/[Rh] value of 0.3 (which in fact corresponds to 0.6 in terms of P/Rh ratio when considering the two phosphorous atoms present in the ligand) appeared enough to achieve well-defined nanoparticles. In this case, larger RhNPs of ca. 1.7 nm were formed (Figure 3). In both cases the nanoparticles were precipitated as black powders by adding cold pentane that contained ca. 66.2 and 45.6% of Rh for $RhPPh_3$ and Rhdppb NPs, respectively (ICP OES analysis). WAXS analysis (Figure 4) in the solid state confirmed the small size of the $RhPPh_3$ NPs with a coherence length of ca. 1.2 nm (close to 1.3 nm determined by TEM) but showed their poorly crystalline character. Moreover, it evidenced that these $RhPPh_3$ NPs do not display a perfect fcc crystalline structure; longer Rh-Rh distances are observed as the result of a strong interaction of the PPh_3 ligand at the metal surface as previously observed with other systems of NPs.[50, 51] For Rhdppb NPs, WAXS analysis (Figure 4) revealed metallic Rh NPs, however the pattern observed in reciprocal space does

not match the expected fcc one. Moreover, coherence length is here also close to 2.2 nm, much larger than the size of 1.7 nm observed by TEM which is counter intuitive since crystalline domains are necessarily smaller than the overall size or equal for single crystalline NPs. Such a behavior was previously observed for metallic NPs elaborated in solution, including Co[52, 53] and Rh,[54] and could be related to a structure primarily observed for the beta phase of manganese (ICSD 41775, PDF 33-887). This less compact structure does not include extended regular planes like the fcc or hcp ones. It is much more difficult to observe and characterize by TEM, which explains the strong discrepancy between the size obtained from TEM and coherence length obtained from WAXS. For the RhPPh$_3$ system, a very broad pattern was observed in the reciprocal space, which cannot be safely attributed to a well-defined structure. Consistently, very few distances are observed in the related RDF. The most likely structure is manganese beta, just like for Rhdppb, with however a much higher disorder.
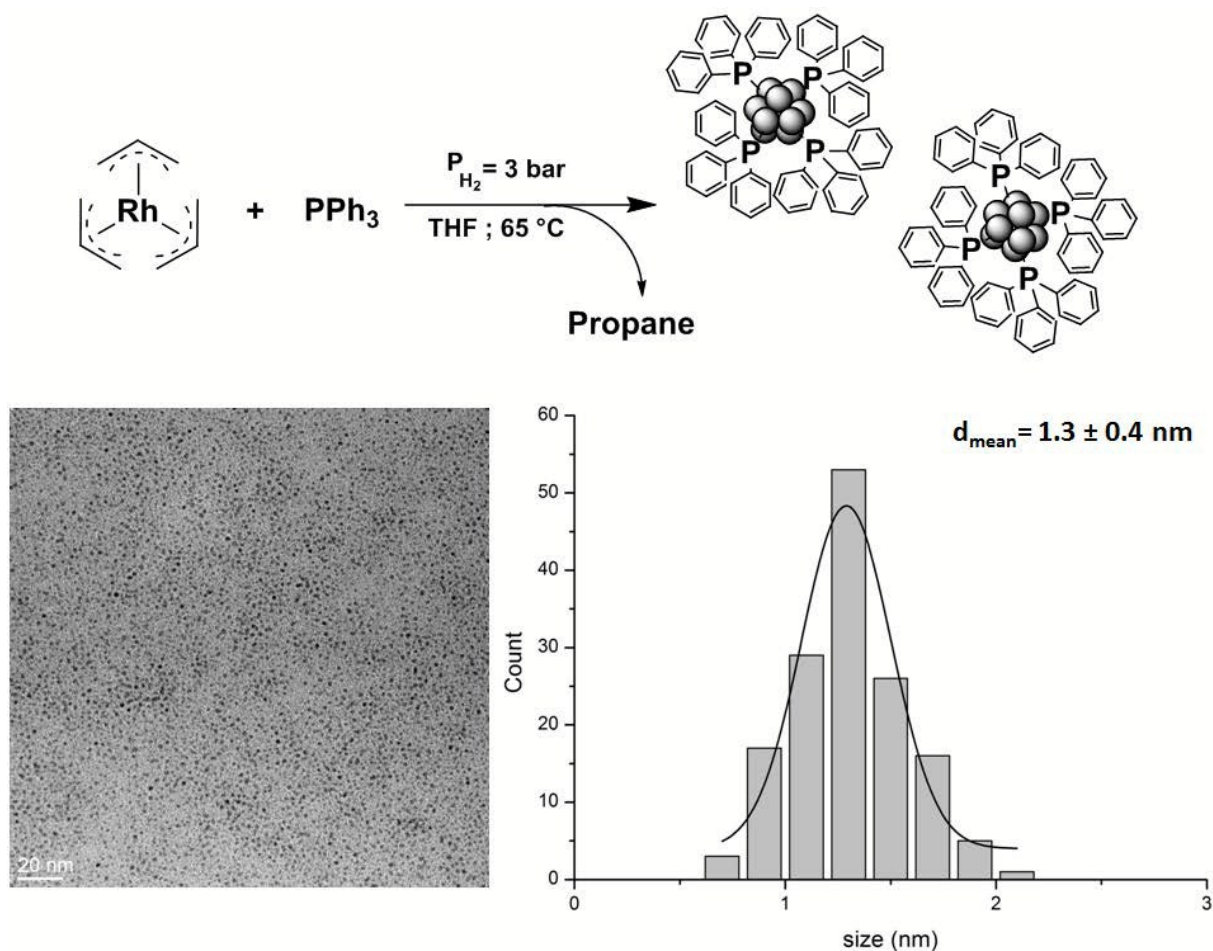
Figure 2. Synthesis, TEM image and size distribution histogram of PPh$_3$-stabilized Rh NPs.
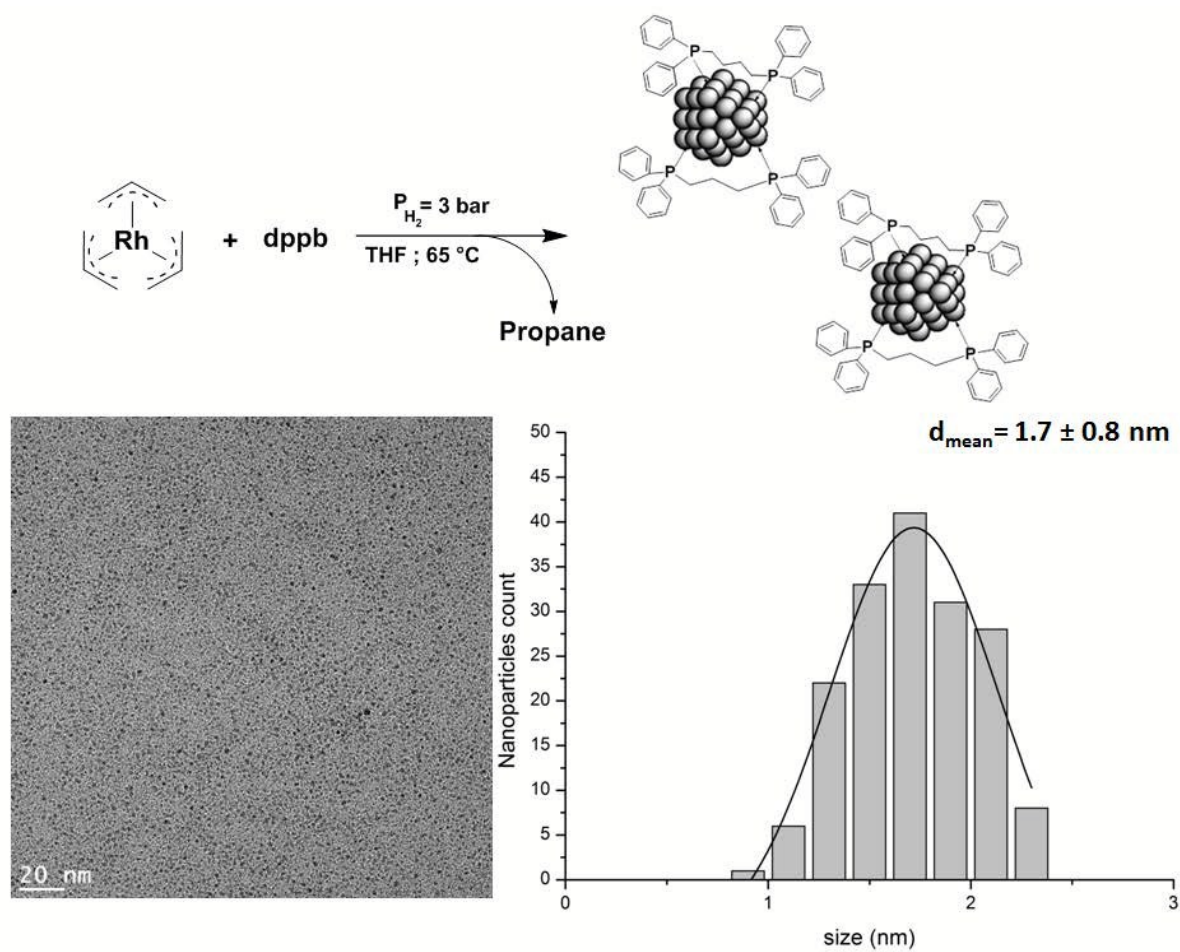

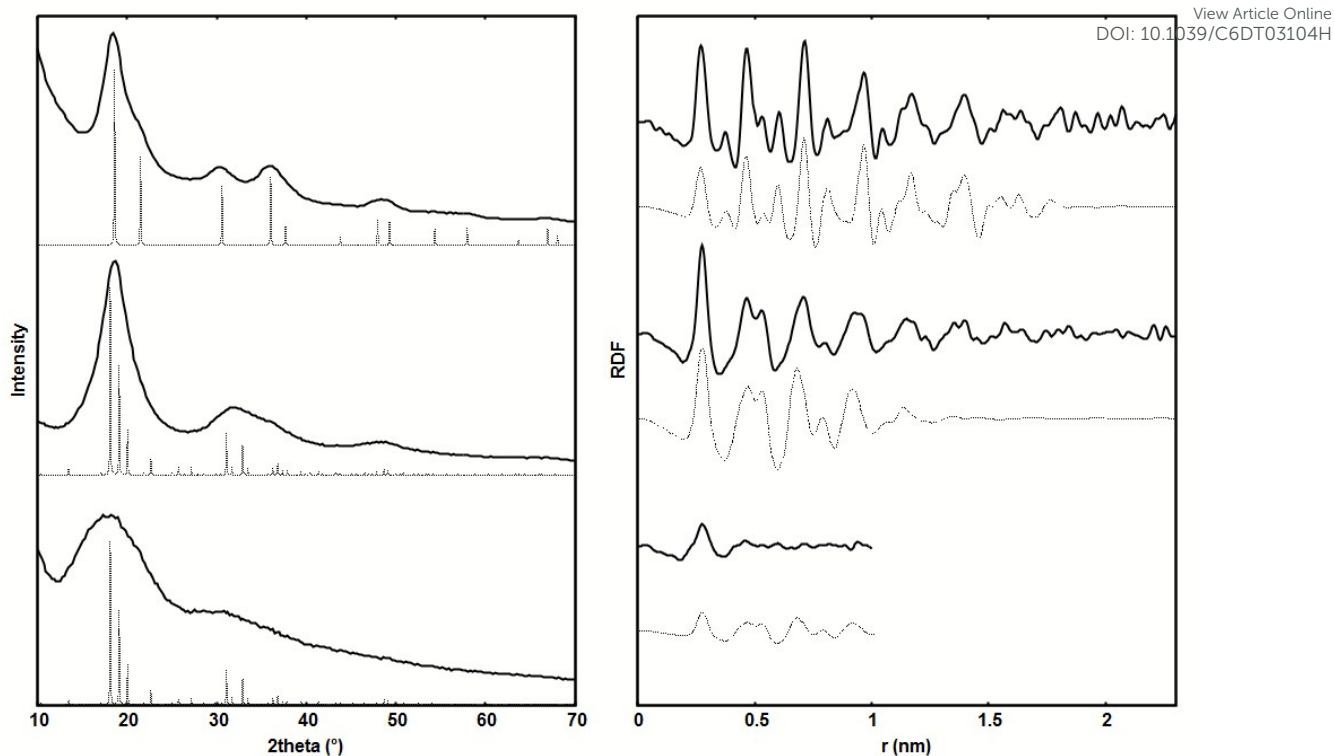**Figure 3**. Synthesis, TEM image and size distribution histogram of dppb-stabilized Rh NPs.

Figure 4. WAXS measurements (solid line) in reciprocal space (left) and real space (right) for RhPVP, Rhdppb and RhPPh$_3$ NPs (from top to bottom) in comparison with calculated data for Rh in the fcc and manganese-β structures (dashed line).

Solution NMR data recorded for RhPPh$_3$ NPs after purification revealed the absence of free phosphine in solution, indicating the strong coordination of the ligand at the metal surface, as previously observed for other phosphine-stabilized nanoparticles. In all cases the Rh NPs were found to be stable for weeks when kept under argon atmosphere.

Deposition of Rh NPs onto magnetic silica support

The Rh NPs previously described were further deposited onto a silica support to obtain the supported catalysts following the method developed by Rossi's group.[43, 55, 12] Amino-functionalized silica-coated magnetite (FFSiNH$_2$) was used as a support and the deposition of the Rh NPs was performed by impregnation of the silica support with a THF solution containing purified Rh NPs under vigorous stirring, at r.t. during 16 h. The THF solutions appeared to be colorless after this deposition step.

Then the solids were washed several times with ethanol to ensure elimination of non-supported nanoparticles. Drying under vacuum led to RhPVP@FFSiNH$_2$, RhPPh$_3$@FFSiNH$_2$ and Rhdppb@FFSiNH$_2$ supported catalysts. The deposition of Rh NPs at the surface of the magnetic support was attested by TEM analysis as shown in Figure 5 for RhPVP NPs. The Rh NPs appeared well-dispersed on the silica shell of the magnetic support, with no aggregation and a mean size close to that observed from colloidal solutions. In the case of phosphine-stabilized systems, TEM analysis did not allow to observe clearly the Rh particles onto the silica support probably due to their smaller mean sizes. ICP OES analysis confirmed in all cases the presence of Rh onto the support.
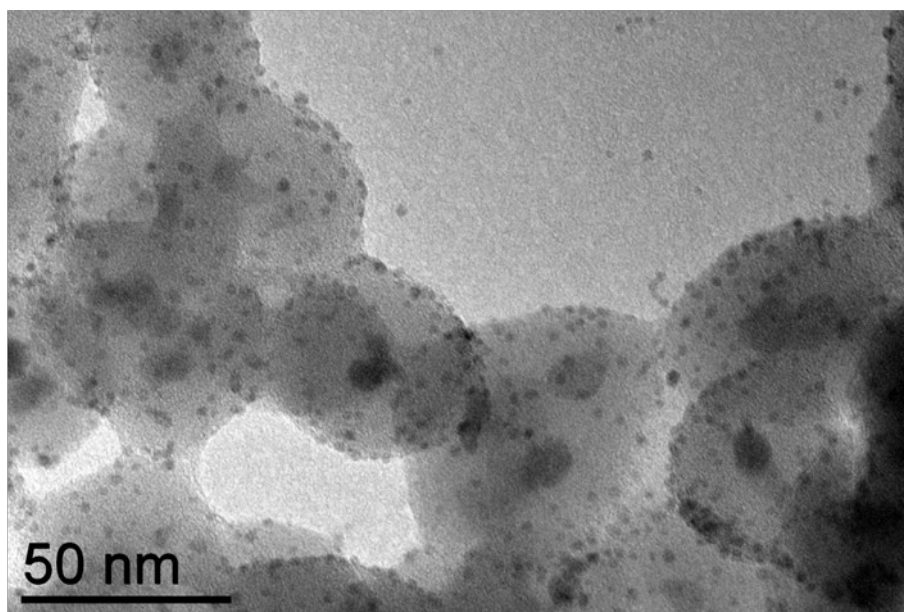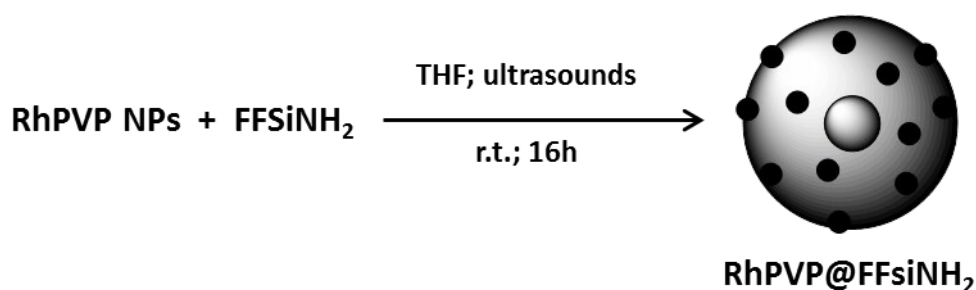

Figure 5. TEM image of RhPVP NPs deposited onto silica-coated magnetite.

Hydrogenation catalysis with non-supported Rh NPs

A first set of hydrogenation catalytic tests was performed using isolated RhPVP, RhPPh$_3$ and Rhdppb NPs and the substrate (cyclohexene) as the liquid phase, following reaction conditions from previous studies.[43, 56] The studies with non-supported Rh NPs were intended to provide with fundamental understanding of the effect of the ligands on activity and stability, but also to serve as a basis for the development of the supported analogues.

During the hydrogenation tests, the temperature was fixed at 75°C and the reaction pressure was maintained constant (6 bar) with the reactor connected to a dihydrogen gas supply tank. The consumption of dihydrogen in the external dihydrogen source was monitored until reaction completion. The final conversion was confirmed by gas chromatography (GC) and the turnover numbers (TONs), expressed in mol of substrate transformed per mol of rhodium, were determined (see ESI, figure S1). From each dihydrogen consumption curve were extracted the following parameters (see Table 1): (a) the period of time with no consumption of dihydrogen before the reaction started, namely induction time; (b) the period of time for reaction completion determined as the time where the consumption of dihydrogen stopped, (c) the turnover frequencies (TOF) determined by the linearization of the hydrogen consumption curves at initial reaction time ($<$ 20% conversion).[57] Considering that 1 mol of substrate is converted per each mol of dihydrogen, the TOF is given first as mol of substrate converted per mol of total rhodium per hour. Knowing that the fraction of exposed Rh atoms (surface atoms) present in each catalyst is different due to their different mean sizes, TOFs corrected by the fraction of surface metal atoms are also given. These corrected TOFs were obtained by dividing the TOFs values by the approximate dispersion (D; the fraction of exposed Rh) values of ca. 0.52, 0.76 and 0.62 for RhPVP, RhPPh$_3$ and Rhdppb, respectively, obtained by considering the formation of full-shell clusters of rhodium and the mean sizes of the Rh NPs determined by TEM analysis. PVP-stabilized Rh NPs exhibited longer induction time and longer reaction time to get full completion than phosphine-stabilized RhNPs, which present very close behaviors. From the corrected TOFs values, the PVP-stabilized Rh NPs are found to be

the most active catalyst. This behavior may be related to the weak interaction of PVP with the

metallic surface, giving rise to a better accessibility of the Rh sites in comparison with a stronger

phosphine Rh-P interaction, which limits the catalytic activity of the phosphine-stabilized Rh NPs.

The longer activation time observed for PVP-stabilized Rh NPs may be due to the lower solubility of

PVP compared to phosphines in cyclohexene, providing an additional steric hindrance on the catalyst

surface. The activity (TOFs) corrected for exposed metal atoms of RhPPh$_3$ and Rhdppb catalysts is

lower than that of RhPVP one, which suggests the phosphine ligands are coordinating strongly to the

metal surface (as observed by NMR studies), blocking active sites. The difference between the two

phosphines is not significant. Given the strong influence of the phosphines on the structure of the

particles as indicated by WAXS data, electronic or faced-directed effects could also intervene.

Table 1. Hydrogenation of cyclohexene with non-supported Rh NPs.[a]

Catalyst	Induction time (h)[b]	Time (h)[c]	TOF (h^{-1})[d]
RhPVP	0.25	2.50	3500 (6730)
RhPPh$_3$	0.07	1.67	3800 (5000)
Rhdppb	0.05	2.14	2800 (4516)

[a] Reaction conditions (solventless): Cyclohexene (29.2 mmol, 2.4 g), Rh catalyst (7.3 μmol), mol substrate/mol catalyst=4000, 75°C, 6 bar of H$_2$.
[b] Time interval without consumption of dihydrogen.
[c] Time interval required for each cycle reaction completion estimated by H$_2$ consumption curves (>99% conversion as determined by GC).
[d] Turnover frequency (TOF) expressed as moles of the substrate transformed per moles of catalyst per h at <20 % conversion. In parenthesis, TOF corrected per mol of surface Rh atoms.

Hydrogenation catalysis with supported Rh NPs

The supported Rh NPs were studied in the same catalysis conditions and the obtained results

are summarized in Table 2. The supported catalysts have the great advantage of being easily

separated magnetically by placing a magnet on the reactor walls. The organic phase is easily

recovered with a syringe for analysis by gas chromatography, while the catalyst can be reused.

Compared with non-supported systems, the $Rh@FFSiNH_2$ catalysts were tested at ca. 10 times

higher substrate to catalyst molar ratio and all of them reached full conversion, with TONs of 36500.

Moreover, for the three supported catalytic systems, the substrate was converted is a shorter period

of time indicating better catalytic performances, which are also corroborated by increased TOFs. For

comparison purpose, the TOFs were corrected for exposed metal atoms. We considered the mean

sizes of the preformed Rh NPs given that the supported catalysts were prepared by impregnation

from the colloidal solutions, and we assumed no evolution in size as shown by TEM. As previously

observed in colloidal conditions, the RhPVP NPs were the most active after immobilization on the

amino-functionalized silica-coated magnetite support and the two other nanocatalysts showed again

no significant difference between the two phosphines. This enhancement in activity and decrease in

the induction time could be explained by elimination of PVP around the Rh cores given the washing

step after deposition of the particles onto the silica support. This may lead to a better accessibility of

the metallic surface. This is not expected with the phosphine-stabilized nanocatalysts due to the

strong Rh-P interaction. The lower TOFs observed for $Rhdppb@FFSiNH_2$ and $RhPPh_3@FFSiNH_2$

compared to $RhPVP@FFSiNH_2$, as for colloidal solutions, support the hypothesis that the phosphine

ligands (PPh_3 and dppb) are still coordinating strongly to the metal surface after immobilization on

silica. The supported phosphine-stabilized systems displayed longer induction times than in the

colloidal (non-supported) analogous, which can be a consequence of using a higher substrate to

catalyst molar ratio (36500 compared to 4000), as seen before for PVA-stabilized Rh NPs.[29]

Table 2. Hydrogenation of cyclohexene with supported Rh NP catalysts.

Catalyst	Induction time (h)[b]	Time (h)[c]	TOF (h^{-1})[d]

RhPVP@FFSiNH$_2$	0.05	0.58	105,700 (203,270)
RhPPh$_3$@FFSiNH$_2$	0.15	1.50	23,650 (31,120)
Rhdppb@FFSiNH$_2$	0.23	1.80	24,850 (40,080)

[a] Reaction conditions (solventless): Cyclohexene (14.6 mmol, 1.2 g), Rh catalyst (0.4 μmol), mol substrate/mol catalyst=36500, 75°C, 6 bar of H$_2$.
[b] Time interval without consumption of dihydrogen.
[c] Time interval required for each cycle reaction completion estimated by H$_2$ consumption curves (>99% conversion as determined by GC).
[d] Turnover frequency (TOF) expressed as moles of the substrate transformed per moles of catalyst per h at 20 % conversion. In parenthesis, TOF corrected per mol of surface Rh atoms.

Taking benefit of the magnetic properties of the support, the catalysts were reused in successive hydrogenation cycles performed by simple application of a magnet on the walls of the reactor. After removing the products and drying the recovered catalyst under vacuum, a new portion of cyclohexene was added in the reactor to pursue the catalysis. Results obtained for 5 successive runs are given in Figure 6 (see also hydrogenation curves in Figure S2-S4, ESI). Interestingly, the initial activity of RhPVP@FFSiNH$_2$ at ca. 200,000 h^{-1} steadily increased until the 5th recycle, reaching ca. 320,000 h^{-1}. An increase of the activity can be explained by a more active surface after the successive reactions probably due to elimination of PVP stabilizer from the nanoparticle's surface. Examples showing activity recovering after removal of stabilizers have been reported before for polymer-stabilized supported metal nanoparticle catalysts.[29, 58] The immobilization of polymer-stabilized Rh NPs is an excellent strategy to retain the high activity of the colloidal NPs, but more importantly it provides a way to improve their catalytic performance as the stabilizer can be removed without compromising their stability. The initial activity of Rudppb@FFSiNH$_2$ and RuPPh$_3$@FFSiNH$_2$ at ca. 40,000 h^{-1} and 30,000 h^{-1}, respectively, increased to 80,000 and 90,000 h^{-1} in the 1st recycle and thus were maintained in this range (50,000 to 100,000 h^{-1}) until the 5th recycle. These results corroborate those found with the colloidal Rh NPs, which suggests that the phosphine ligands are coordinating strongly to the metal surface and, moreover, they are not being displaced during the recycling experiments.
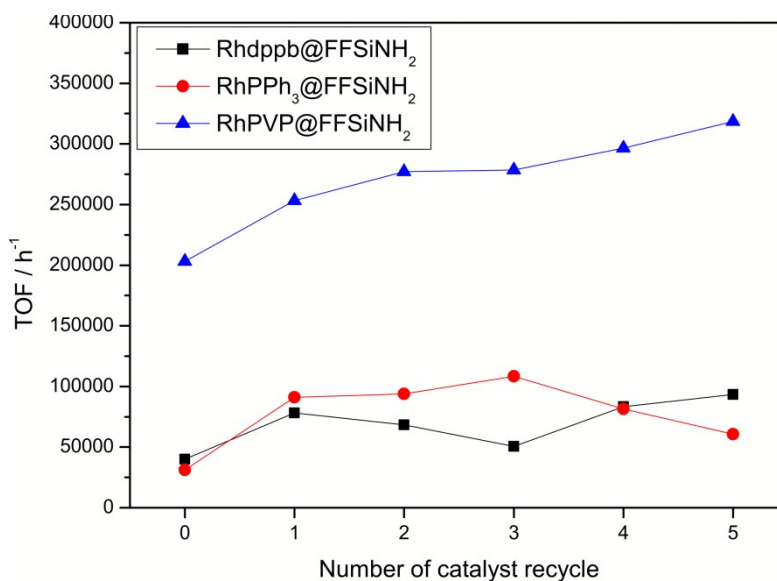
Figure 6. Catalyst recycling test expressed as TOF (h^{-1}, corrected for exposed Rh atoms) of Rhdppb@FFSiNH$_2$ (squares), RhPPh$_3$@FFSiNH$_2$ (circles) and RhPVP @FFSiNH$_2$ (triangles) for 5 successive hydrogenation runs of cyclohexene.

Conclusion

Here we compared the surface reactivity of Rh NPs stabilized either by a polymer or a phosphine ligand when involved in a model catalytic reaction namely, cyclohexene hydrogenation. For that purpose, well-defined and very small Rh NPs were achieved from solution organometallic synthesis using [Rh(η^3-C$_3$H$_5$)$_3$] as metal source and a polymer (PVP), a monophosphine (PPh$_3$) and a diphosphine (dppb) as stabilizers that displayed mean sizes of 2.2, 1.3 and 1.7 nm, respectively. PVP-stabilized Rh NPs was the most active catalyst. This can be attributed to a more accessible metallic surface due to weak interaction between PVP and Rh surface atoms compared to phosphine-stabilized nanoparticles where the phosphines are strongly coordinated at nanoparticle surfaces. No significant difference was observed between the two phosphines indicating that there is a similar blocking of surface rhodium atoms by the ligand whatever a mono- or bidentate coordination mode. However, electronic or facet-directed effects induced by the phosphine ligands cannot be ruled out.

21

Dalton Transactions Accepted Manuscript

The deposition of the Rh NPs onto amino-functionalized silica-coated magnetite as a support by simple impregnation method led to supported Rh catalysts with homogeneous dispersion of the particles all over the support. The supported nanocatalysts were also tested in cyclohexene hydrogenation in similar reaction conditions as colloidal particles and showed better catalytic performances. Again, the silica-supported RhPVP NPs were the most active catalyst and no difference was observed between the PPh$_3$ and dppb ligands. This indicates that the phosphine ligands are still coordinating strongly to the metal surface after immobilization of the particles and limit the catalysis act. Moreover, taking advantage of the magnetic properties of the support, the catalysts could be reused easily in successive hydrogenation cycles. In the case of RhPVP@FFSiNH$_2$, a more active surface was obtained after the successive reactions probably due to elimination of PVP from the Rh NPs. The immobilization of PVP-stabilized Rh NPs appeared thus to be an excellent strategy to retain and even improve the catalytic performance of the NPs as the polymer can be removed without compromising their stability. The results obtained with Rhdppb@FFSiNH$_2$ and RhPPh$_3$@FFSiNH$_2$ nanocatalysts corroborated those observed with the colloidal Rh NPs, which suggests that the phosphine ligands are coordinating strongly to the metal surface and, moreover, they are not being displaced during their immobilization as well as the recycling experiments.

In summary, this work evidenced the interest of the organometallic approach for the preparation of very small and stable rhodium nanoparticles having different surface properties as well as the advantage of using an amino functionalized silica-coated magnetite support for their immobilization. In comparison with PVP polymer the use of phosphines as stabilizing ligands gave rise to the formation of smaller nanoparticles but also to less active nanocatalysts. This can be attributed as the result of a strong coordination of the ligand at the metal surface that blocks some surface atoms and limits the reactivity of the metallic surface even after several recycling of the supported

nanocatalysts. This work illustrates well the compromise that is needed between size and surface

control to develop metal nanocatalysts.

Acknowledgements

References

1 *Physics and Chemistry of Metal Cluster Compounds*, ed. L.J. de Jongh, Kluwer Academic Publishers, Dordrecht, 1994.

2 *Introduction to Nanotechnology, in Nanoscale Materials in Chemistry*, ed. K.J. Klabunde, John Wiley & Sons, Inc, 2001.

3 *Nanoparticles: From Theory to Application*, ed. G. Schmid, 2nd Ed., Wiley-VCH, Weinheim, 2012.

4 *Concepts in Nanocatalysis*, eds. K. Philippot and P. Serp, Wiley-VCH, Weinheim, 2013.

5 *Nanocatalysis*, eds. U. Heiz and U. Landman, Springer, 2007.

6 *Nanoparticles in catalysis*, ed. D. Astruc, Wiley-VCH Weinheim, 2008.

7 *Metal Nanoparticles for Catalysis: Advances and Applications*, ed. T. Tao, RSC, 2014.

8 H.-J. Freund and G.A. Somorjai, *Catal. Lett*., 2015, **145**, 1-2.

9 J.E. Mondloch, E. Bayram and R.G. Finke, *J. Mol. Catal. A: Chemical*, 2012, **355**, 1-38.

10 F. Schüth, *Angew. Chem. Int. Ed*., 2014, **53**, 8599-8604.

11 M.J.L. Tschan, O. Diebolt and P.W. N. M. van Leeuwen, *Top. Catal*., 2014, **57**, 1054-1065.

12 N.J.S. Costa and L.M. Rossi, *Nanoscale*, 2012, **4**, 5826-5834.

13 Y. Yuan, N. Yan and P.J. Dyson, *ACS Catalysis*, 2012, **2**, 1057-1069.

14 L. Yin and M. A. El-Sayed, *J. Phys. Chem. B*, 2001, 8938-43.

15 R.R. Dykeman, N. Yan, R. Scopelliti and P.J. Dyson , *Inorganic chemistry*, 2011, 50 (3),717-719.

16 D. Gonzalez-Galvez, P. Nolis, K. Philippot, B. Chaudret, P. van Leeuwen, *ACS Catalysis*, 2012, 2 (3) 317-321.

17 S. A. Stratton, K. L. Luska and A. Moores. *Catalysis Today*, 2012, 183(1), 96-100.

18 B.L. Cushing, V.L. Kolesnichenko and C.J. O'Connor, *Chem. Rev*., 2004, **104**, 3893-3946.

19 C. Amiens, B. Chaudret, D. Ciuculescu-Pradines, V. Colliere, K. Fajerwerg, P. Fau, M. Kahn, A. Maisonnat, K. Soulantica and K. Philippot, *New J. Chem*., 2013, **37**, 3374-3401.

20 C. Amiens, D. Ciuculescu-Pradines and K. Philippot, *Coord. Chem. Rev*., 2016, **38**, 409-432.

21 S. Kinayyigit and K. Philippot, in *Metal Nanoparticles for Catalysis: Advances and Applications*, RSC, 2014, 47-82.

22 M. M. Guerrero; N. J. S.Costa,; L. L.R.Vono; L.M. Rossi,; E.V. Gusevskaya and K. Philippot, *J. Mater. Chem*. A, 2012, **1**, 1441-1149.

23 N.J.S. Costa, R.F. Jardim, S.H. Masunaga, D. Zanchet, R. Landers and L.M. Rossi, *ACS Catalysis*, 2012, **2**, 925-929.

24 A. Gual, C. Godard, S. Castillón and C. Claver, *Dalton Trans.*, 2010, **39**, 11499-11512.

25 D. J. Snelders, N. Yan, G. Laurency and P. J. Dyson, *ACS Catal.*, 2012, **2**, 201-207.

26 S. Xie, X. Liu and Y. Xia, *Nano Research*, 2015, **8**, 82-96.

27 A. Roucoux and K. Philippot, in *Handbook of Homogeneous Hydrogenation*, eds. J. G de Vries and C. J. Elsevier, Wiley-VCH, 2007, 217-255.

28 M. Guerrero, N. T. Than Chau, S. Noël, A. Denicourt-Nowicki, F. Hapiot, A. Roucoux, E. Monflier, K. Philippot, *Curr. Org. Chem.*, 2013, **17**, 364-399.

29 L.M. Rossi, L.L.R. Vono, M.A.S. Garcia, T.L.T. Faria and J.A. Lopez-Sanchez, *Topics in Catalysis*, 2013, **56**, 1228-1238.

30 M. Zahmakiran and S. Ozkar, *Appl. Catal. B*, 2009, **89**, 104-110.

31 Z. Nazarpoor, K. Khivantsev, E. Kyriakidou, C. Kubicki, S. Ma, P.T. Fanson, O.S. Alexeev and M.D. Amiridis, *J. Coll. Int. Sc.*, 2013, **398**, 22-32.

32 M.A,S. Garcia, K.C.B. Oliveira, J.C.S. Costa, P. Corio, E.V. Gusevskaya, E.N. dos Santos and L.M. Rossi, *Chem. Cat. Chem*, 2015, **7**, 1566-1572.

33 J. A. Widegren and R. G. Finke, *Inorg. Chem.*, 2002, **41**, 1558–1572.

34 J.D. Aiken III and R.G. Finke, *J. Mol. Catal. A: Chem.*, 2003, **191**, 187-207.

35 K.H., Park, K. Jang, Kwonho, H.J. Kim, Hae Jin and S. Uk Son, Seung, *Angew. Chem. Int. Ed.*, 2007, **46,** 1152-1154.

36 J.-L. Pellegata, C. Blandy, V. Collière, R. Choukroun, C. Pan, K. Philippot and B. Chaudret, *J. Mol. Catal. A: Chemical*, 2002, **178,** 55-61.

37 D. Wostek-Wojciechowska, J.K. Jeszka, C. Amiens, B. Chaudret and P. Lecante, *J. Coll. Int. Sc.* 2005, 1, **287**, 107-113.

38 M. Rosa Axet, S. Castillón, C. Claver, K. Philippot, P. Lecante and B. Chaudret, Eur. *J. Inorg. Chem.*, 2008, 3460-3466.

39 M.V. Escárcega-Bobadilla, C. Tortosa, E.Teuma, C. Pradel, A. Orejón, M. Gómez and A.M. Masdeu-Bultó, *Catal. Today*, 2009, 3, **148**, 398-404.

40 J. Llop-Castelbou, E. Bresó-Femenia, P. Blondeau, B. Chaudret, S. Castillón, C. Claver and C. Godard, *Chem. Cat. Chem.* 2014, **6**, 3160-3168.

41 J. Zhang; M. Ibrahim; V. Collière; H. Asakura; T. Tanaka; K. Teramura; K. Philippot and N. Yan, *J. Mol. Catal. A.* 2016, (doi.org/10.1016/j.molcata.2016.01.014).

42 R. Beckhaus, in *Synthetic Methods of Organometallic and Inorganic Chemistry*, Vol. 9, ed. W.A. Herrmann, New York, 2000, 38.

43 M.J. Jacinto, P.K. Kiyohara, S.H. Masunaga, R.F. Jardim and L.M. Rossi, *Appl. Catal. A: General* 2008, **338**, 52-57.

44 D. Zitoun, M. Respaud, M.C. Fromen; M.J. Casanove, P. Lecante, C. Amiens, B. Chaudret, *J. Phys. Chem. B*, 2003, **107**, 6997-7005.

45 PhD E. Ramírez Meneses, UPS-Toulouse, 2004.

46 N. Atamena, D. Ciuculescu, G. Alcaraz, A. Smekhova, F. Wilhelm, A. Rogalev, B. Chaudret, P. Lecante, R. E. Benfield and C. Amiens, *Chem. Commun.*, 2010, **46**, 2453-2455.

47 P. Lara, K. Philippot and B. Chaudret, *Chem. Cat. Chem.*, 2013, **5**, 28-45.

48 S. Kinnayyigit, P. Lara, P. Lecante, K. Philippot and B. Chaudret, *Nanoscale*, 2014, **6**, 539-546.

49 J. Osuna, D. de Caro, C. Amiens, B. Chaudret, J ; Phys. Chem. C, 1996, 100, 14571-14574.

50 F. Dassenoy, K. Philippot, T. Ould Ely, C. Amiens, P. Lecante, E. Snoeck, A. Mosset, M.-J. Casanove and B. Chaudret, *New J. Chem.*, 1998, 703-711.

51 E. Ramirez, S. Jansat, K. Philippot, P. Lecante, M. Gómez, A. Masdeu and B. Chaudret, *J. Organomet. Chem.*, 2004, **689**, 4601-4610.

52 D. P. Dinega and M. G. Bawendi, *Angew. Chem. Int. Ed.* 1999, **38**, 1788-1791.

[53] F.Dassenoy, M.-J. Casanove, P. Lecante, M. Verelst, E. Snoeck, A. Mosset, T. Ould-Ely, C. Amiens and B. Chaudret, *J. Chem. Phys*., 2000, **12**, 8137-8145.

[54] R. Choukroun, D. de Caro, B. Chaudret, P. Lecante and E. Snoeck, *New J. Chem*., 2001, **25**, 525-527.

[55] M.J. Jacinto, F.P. Silva, P.K. Kiyohara, R. Landers and L.M. Rossi, *Chem.Cat.Chem.* 2012, **4,** 698-703.

[56] C.H. Pélisson, L.L.R. Vono, C. Hubert, A. Denicourt-Nowicki, L.M. Rossi and A. Roucoux, *Catalysis Today*, 2012, **183**, 124-129.

[57] A. P. Umpierre, E. de Jesús and J. Dupont, *Chem. Cat. Chem.* 2011, **3**, 1413-1418.

[58] J. A. Lopez-Sanchez, N. Dimitratos, C. Hammond, G. L. Brett, L. Kesavan, S. White, P. Miedziak, R. Tiruvalam, R. L. Jenkins, A. F. Carley, D. Knight, C. J. Kiely and G. J. Hutchings, *Nature Chem*., 2011, **3**, 551-556.